CrossMark

Microbiologically induced concrete corrosion: A case study from a combined sewer network

C. Grengg [a,*], F. Mittermayr [b], A. Baldermann [a], M.E. Böttcher [c], A. Leis [d], G. Koraimann [e], P. Grunert [f,g], M. Dietzel [a]

[a] Institute of Applied Geosciences, Graz University of Technology, Rechbauerstraße 12, 8010, Graz, Austria
[b] Institute of Technology and Testing of Building Materials, Graz University of Technology, Inffeldgasse 24, 8010, Graz, Austria
[c] Leibniz Institute for Baltic Sea Research (IOW), Seestraße 15, D-18119 Warnemünde, Germany
[d] RESOURCES—Institute for Water, Energy and Sustainability, 8010, Graz, Austria
[e] Institute of Molecular Biosciences, Graz Karl-Franzens University, Humboldstraße 50, 8010, Graz, Austria
[f] Institute of Earthsciences, Graz Karl-Franzens University, Heinrichstraße 26, 8010, Graz, Austria
[g] Department of Earth and Planetary Sciences, Rutgers University, 610 Taylor Road, Piscataway, NJ 08854-8066, USA

ARTICLE INFO

ABSTRACT

In this study, a strongly deteriorated concrete-based sewer system was investigated by using a multi proxy approach based on gaseous, hydro-geochemical, microbiological, mineralogical and mechanical analyses. Therefore, gas, liquid, and solid samples were taken throughout the entire sewer system. Long term measurements of gaseous hydrogen sulfide (H_2S) within the sewer atmosphere yielded concentrations up to 367 ppm. Interstitial fluids, extracted from deteriorated concrete by squeezing, contained sulfate (SO_4^{2-}) concentrations of up to 104 g l^{-1} at strong acidic conditions ($0.7 > pH > 3.1$) and are close to the saturation state of gypsum. This sulfuric acid attack is indicative for a well-established biofilm containing sulfide oxidizing bacteria (SOB), which was analyzed to consist mainly of *Acidithiobacillus thiooxidans*. The micro-structure of the attacked concrete displays a progressing alteration zone, which is caused by microbially induced concrete corrosion (MICC), with a suggested pH gradient from about 13 to <1, from the intact inner concrete zone to the outermost heavily deteriorated concrete. Calcium sulfate minerals such as gypsum ($CaSO_4 \cdot 2H_2O$), bassanite ($CaSO_4 \cdot 1/2H_2O$) and anhydrite ($CaSO_4$) are abundant in the altered concrete, which were formed from the dissolution of the cement phases and Ca-bearing aggregates. Remarkably high corrosion rates of different precast concrete manholes were quantified to reach values greater than 1 cm yr^{-1}, despite the fact that C_3A-free cement, fly ash and a w/c of ~0.35 was used.

© 2015 Elsevier Ltd. All rights reserved.

1. Introduction

Corrosion of concrete-based sewer systems due to the emission of hydrogen sulfide (H_2S) from wastewater is a worldwide occurring issue with great economical relevance. The so-called microbially induced concrete corrosion (MICC) [1,2] is considered to significantly reduce the lifespan of concrete structures, from expected 100 down to 30–50 years, in extreme cases even down to 10 years [3]. The required remediation actions are often challenging as individual processes linked to MICC still remain uncertain and thus typically generate high costs. It has been estimated in 2002 that the United States need to spend about 390 billion dollars within the following 20 years in order to keep the existing wastewater infrastructure on life support [1]. In 1996, over 520 million dollars were spent solely in Los Angeles County for restorations of corroded sewer systems, which were directly assigned to MICC [4]. Besides economic aspects, H_2S and other volatile components such as ammonia

(NH_3), which both are common byproducts of MICC, are extremely toxic even in low concentrations and can cause significant health related consequences [5,6]. Additionally, H_2S features an extremely low odor threshold of 0.0035 ppm, thus often being subject to community appeals due to emerging odor problems [7]. Although, the earliest studies of MICC date back to 1900 [8] the environmental controls, processes, and corrosion rates of MICC are still in debate.

The deterioration of concrete that is subjected to MICC is attributed to a chain of complex biotic and abiotic chemical reactions: (i) Sulfate-reducing bacteria (SRB), e.g. *Desulfovibrio spp.* and *Desulfomaculum spp.* [9,10], develop in the organic-rich wastewater and colonialize the adjacent sewer walls and sediment layers. The SRB colonize within an anaerobic biofilm, wherein organic matter breaks down and sulfate is progressively reduced to gaseous H_2S [11]. (ii) Accordingly, H_2S degases into the sewer atmosphere and subsequently accumulates in the pore space of the concrete via gaseous diffusion and subsequent absorption in the interstitial solution. Since concrete made with ordinary Portland cement (OPC) is a strongly alkaline media with an average pH value of ~13.5 in the pore solution [12], chemical acid-base reactions such as

* Corresponding author.
E-mail address: cyrill.grengg@tugraz.at (C. Grengg).

carbonation and in particular H_2S acidification successively cause the pH to drop. Starting from pH 9.5, progressive colonization of the concrete walls with strains of sulfur-oxidizing bacteria (SOB) occurs. SOB use H_2S either directly [13] or via different key precursors, e.g. thiosulfate (S_2O_3) or elemental sulfur (S^0) as an electron donor [14]. These reactions finally result in the formation of sulfuric acid (H_2SO_4), which attacks the concrete and leads to a variety of dissolution processes, besides enhancing some neo-formation reactions of sulfate mineral phases within the cementitious matrix [15,16]. (iii) The dissociation of H_2SO_4 goes almost to completion and thus strongly reduces the pH for stimulating the dissolution of silicate, hydroxide and carbonate minerals. In addition, by providing SO_4^{2-} the precipitation of sulfate minerals such as gypsum ($CaSO_4 \cdot 2H_2O$) and ettringite (($CaO)_3 \cdot Al_2O_3 \cdot (CaSO_4)_3 \cdot 32H_2O$) is promoted [17,18]. The formation of gypsum and ettringite is well known to cause intense microstructural damage by high crystallization pressures [19–21]. (iv) As the interstitial solution pH of the initially damaged concrete decreases progressively, different strains of bacteria colonize the pores of the concrete, with *Acidithiobacillus thiooxidans* being the most aggressive one [10].

Many laboratory studies were carried out focusing on the deterioration mechanisms related to MICC on different types of concrete [1,15, 22–24], but so far field studies on MICC are rare [25]. Although, the results from laboratory experiments have been widely used to draw conclusions about MICC processes in natural environments, it is almost impossible to reproduce field environmental conditions of MICC in the lab. The aim of the present case study is to contribute to a deeper understanding of reaction paths, environmental controls, and corrosion rates related to MICC in a modern Austrian sewer system by introducing an advanced multi proxy approach that comprises gaseous, hydro-geochemical, bacteriological, mineralogical and mechanical analyses.

2. Study site

The investigated sewer system is located mainly in rural areas near the city of Graz in the south-eastern part of Austria. It can be categorized as a combined sewer network [26], thus transporting the daily wastewater of around 13,000 citizen as well as the runoff from seasonal storm events. In recent years, the Austrian government demanded the fusion of smaller wastewater systems, which resulted in increasing amounts of longer intercepting sewers. Consistent with this concept, two new power mains were installed in 2004 in order to secure proper wastewater transport in local communities.

The newly built sewer system comprises a concrete storage basin (SB1), where the wastewater from the surrounding sewer channels is collected and pumped through the first power main (PM1), on average, every six hours. The PM1 is made of cast iron and polyethylene (PE) insets, with a sewer diameter of 200 mm and a sewer length of 4 km. The adjoining PE gravity sewer (GS1), consists of around 50 concrete-based manholes (GS1-1 to GS1-50) and two small income pipes of residential areas, and is about 5 km in length. Subsequently, the wastewater is collected within a second storage basin (SB2) from which it is continuously pumped into another power main (PM2), with a length of 1.8 km and a 300 mm sewer diameter. The last part of the system holds another gravity sewer section (GS2), comprising 30 concrete-based manholes (GS2-1 to GS2-30), before the wastewater finally reaches the purification plant (Fig. 1).

Both storage basins (SB1 and SB2) are made of concrete; however, no further investigations were conducted on this material since they showed no signs of visual damage. In contrary, some of the manholes in the gravity sewers were strongly deteriorated. In severe cases, the first few centimeters of the concrete revealed a mushy appearance and could be easily scraped off with bare hands. With increasing
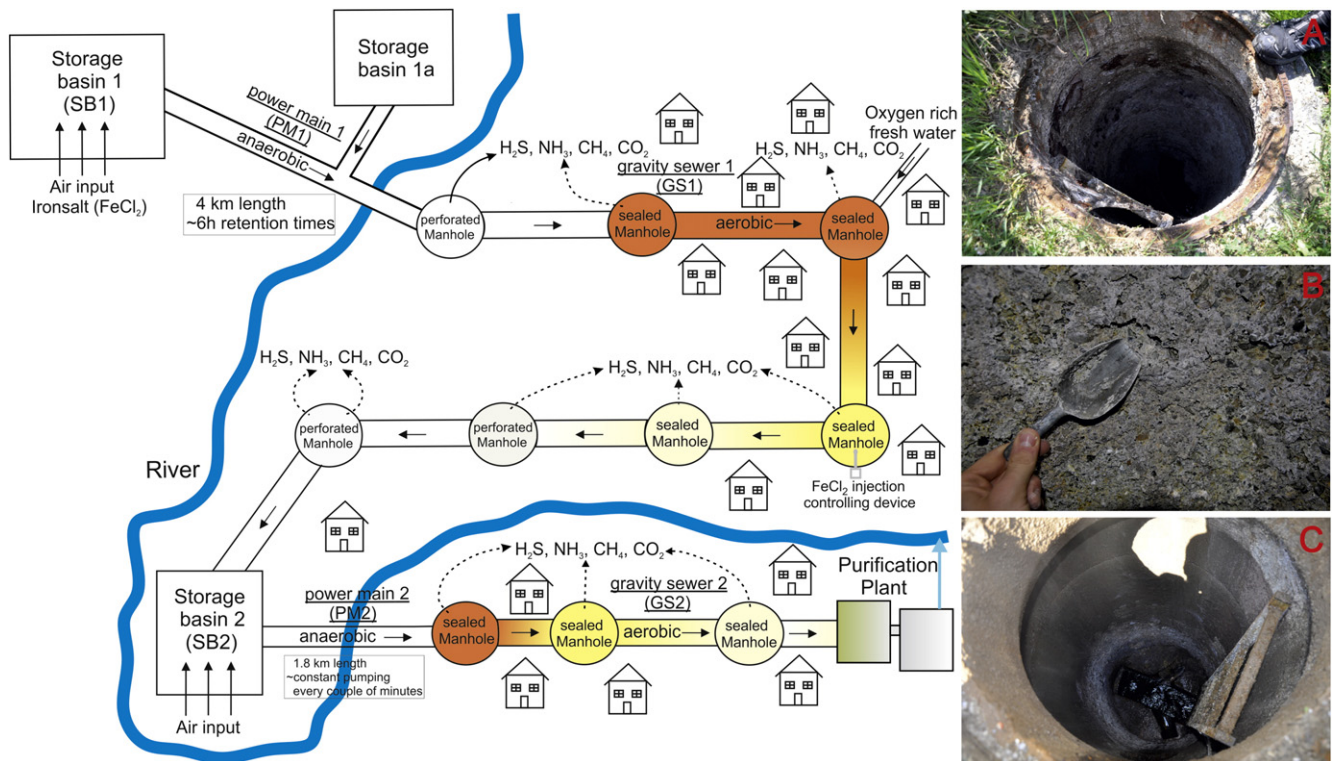
Fig. 1. Schematic map of the Austrian sewer network near Graz. The intensity of concrete corrosion is indicated by the orange (intense deterioration) and yellow color (less deterioration). Note that the highest corrosion level occurs within the sealed manhole covers. Intensive degassing of H_2S, CO_2, CH_4, and NH_3 is indicated with solid arrows within the upper parts of the system and the partly perforated manhole covers, while lower emission is indicated with doted arrows. Fresh air and iron-salt ($FeCl_2$) are constantly added to the storage basin 1 (SB1) to limit the H_2S concentrations in the atmosphere of the selected manholes by iron sulfide formation. On the right, inserted images A and B show examples of strongly deteriorated concrete of manholes within the upper parts of the gravity sewer sections, while C represents less degraded concrete of manholes within the middle parts of the system.

distance from the power main outlets, the intensity of concrete corrosion decreases, as seen in non-corroded manholes at the end of these sections (see Fig. 1, A–C). The manholes are between 30 cm and 400 cm deep with great majority at an average depth of about 200–300 cm, and consist of precast concrete elements. The contract document specified precast elements with a compressive strength class of C30/37, C_3A free cement and a minimum water/cement (w/c) ratio of 0.45 to withstand severe aggressive environments (AS2 according to ÖNORM B 2503: Drain and sewer systems—Supplementary specifications for design, construction and testing). This classification corresponds to exposure class XA2 for chemical attack according to ÖNORM B 4710-1 (Concrete—Part 1: Specification, production, use and verification of conformity. Rules for the implementation of EN 206-1 for normal and heavy concrete). According to the precast factory, implemented elements possessed a w/c ratio of ~0.35. CEM I 42.5 N (C_3A-free) plus fly ash and 0.25 wt. % of a PCE based superplasticizer, referred to cement content, were added to the concrete mixture.

The transported wastewater comprises mainly domestic wastewater, although one surface quarry and some minor commercial areas are also discharging into the system. Nevertheless, both the quality and the chemical composition of the wastewater fulfill the statutory requirements for communal wastewater. Since the new power mains were installed, community complains of odor rose, which were caused by constant H_2S emission from the sewer system (Fig. 1). As a first countermeasure, the manhole covers in populated areas were sealed, whereas the sewer sections in sparsely populated regions remained perforated. Secondly, in order to prevent the establishment of anaerobic conditions (and subsequently H_2S accumulation) within the power mains, fresh air is pumped into the storage basins. Thirdly, a 15% iron(II)chloride ($FeCl_2$) solution is added regularly into the primary storage basin (since 2010) in order to reduce H_2S formation [20] by precipitation of sulfide ions as iron sulfides (e.g., pyrite, FeS_2, and ironmonosulfide, FeS).

3. Materials and methods

In total 84 samples were collected for this study. This comprises solid and liquid samples (58 in total) from the corroded manholes of GS1 and GS2, as well as, liquid samples of SB1 and SB2 (5 in total). Gas measurements were conducted during the six sampling dates within representative manholes to value the concentrations of H_2S, CO_2, and CH_4. In addition, long term gas observations were carried out in order to determine variations in the total H_2S volumes. Drill cores (21 in total), of 5 cm in diameter, were taken from heavily damaged and intact concrete to evaluate the concrete composition and corrosion rates. The residual thickness of the altered concrete liner was directly measured and compared with that of unaltered concrete (initially about 13 cm thick) to achieve corrosion rates in cm yr^{-1}.

3.1. Solids

Deteriorated concrete mush from different sites was sampled and shoveled into plastic bags. The samples were dried at 40 °C and subsequently grounded in a McCrone micronizing mill for 8 min, together with 10 wt.% ZnO as internal standard. X-ray diffraction (XRD) patterns of randomly oriented preparations were recorded over the range of 4–85°2Θ with a step size of 0.008°2Θ and a count time of 40 s/step, using a PANalytical X'Pert PRO diffractometer. The diffractometer was equipped with a Co-tube (40 kV and 40 mA), a spinner stage, 0.5° divergence and antiscattering slits, and a Scientific X'Celerator detector. Mineral identification and quantification were carried out based on Rietveld refinement of powder XRD patterns using the PANalytical X'Pert HighScore software (version 2.2e) and pdf-2 database.

Extracted drill cores were used for compressive strength and gross density analysis. Therefore, 5 cm cylinders were cut (non-damaged part), subsequently dried, plane-parallel polished and tested, using a Toni Technik 300 kN testing machine, according to Austrian guidelines

ÖNORM EN 12504-1 (Testing concrete in structures—Part1: Cored specimens—Taking, examining and testing in compression).

In order to study mineral alterations and neo-formation features of the concrete, selected samples were analyzed with a Zeiss DSM 982 Gemini scanning electron microscope (SEM), operated at 5 kV accelerating voltage, by mounting the samples on standard SEM stubs. Images of the sample material have been taken by using the DISS 5 software package (version 5.9.9.1). In addition, polished thin sections of various drill core samples were prepared to study the microstructural damage of the concrete by combined back-scattered electron imaging (BSE) and single spot analyses using an electron microprobe (EMPA) JEOL JXA-8200 Superprobe. Single spot analyses were made at an accelerating voltage of 15 kV and 5 nA.

Damaged and unaltered concrete samples were analyzed for their sulfur (S) and total organic carbon (TOC, after acidification of samples to remove carbonate) contents using a Leco CS230 analyzer. The analytical error is <5%.

3.2. Liquids

On site, pH and electric conductivity (EC) were measured using a WTW Multi350i instrument equipped with a SenTix41 and a TetraCon325 electrode. O_2 concentrations and redox potential were measured using a Hach LDO and a SenTix ORP electrode, respectively. For further hydrochemical analyses, wastewater samples were taken throughout the whole sewer system.

In the laboratory, the liquid samples were centrifuged using an Avanti™-J-25I centrifuge and subsequently filtered through 0.45 μm membranes to remove suspended solids and most of the colloidal fraction. Afterwards, the carbonate alkalinity was measured by potentiometric titration with 0.005 M HCl (analytic error < 3%). The major, minor, and trace element concentrations of filtered samples was measured by a Dionex ICS-3000 ion chromatograph (IC) and a PerkinElmer Optima 8300DV inductively coupled plasma optical emission spectrometer (ICP-OES; samples acidified with 2% HNO_3). The analytic error was determined to be < 3% for IC and < 6% for ICP-OES analyses. The dissolved organic carbon content (DOC) was analyzed using a Shimadzu TOC-VcPH + ASI-V Analyzer, with an analytical error below 5%.

Dissolved H_2S was preserved with 5% Zn acetate solution and directly measured spectrophotometrically at Leibniz Institute for Baltic Sea Research Warnemünde (IOW) according to Cline (1969) [27] using a Specord 40 (Analytic Jena) device with an analytical precision of ± 2% [28].

Hydrochemical modelling was carried out using the computer code PHREEQCi (version 3.1.5-9133). The minteq database was applied in order to calculate the saturation indices of gypsum and anhydrite, whereas the llnl database was used for bassanite [29].

A hydraulic press, in a modified setup of Tritthart [12], was used to extract the interstitial solutions of the concrete. Therefore, between 800 and 1100 g of the deteriorated concrete was filled into a steel cylinder of a specially adapted press and pressurized at ~1200 kN/mm². The squeezed solutions were sucked into a syringe. Conductivity and pH measurements were conducted instantly after sampling. The extracted pore solutions were then filtered through a 0.45 μm membrane filter, and analyzed with the methods described above (see more details [30]).

3.3. Microbiological analyses

The samples were analyzed to prove the existence of SOB in the sampled concrete. 1 g of deteriorated concrete was suspended in 1 ml 0.9% NaCl solution. 0.5 ml was used to inoculate a 100 ml Erlenmayer flask containing 20 ml of modified growth medium for the enrichment of Thiobacilli [31]. The medium contained $(NH_4)_2SO_4$ (0.4), KH_2PO_4 (0.4), $CaCl_2$ (0.25), $FeSO_4$ (0.01), $MgSO_4$ (0.5) and $Na_2S_2O_3$ (5) salts, reported in g l^{-1}, that were dissolved in distilled water. Bacteria, growing in this medium in a shaker–incubator at 25 °C for five to seven days,

were plated on a solid medium with the same composition, but additionally containing 1.5 g l^{-1} agar. Bacterial cells harvested by centrifugation from the liquid cultures or from colonies that were suspended in 50 μl water were used to extract DNA. The samples were subjected to heat induced lysis for 10 min at 98 °C. The released DNA was used for amplification of a 298 base pair 16S rDNA fragment using primers in conserved regions flanking two highly variable regions V5 and V6 [32] in standard PCR reactions using Phusion DNA polymerase (New England Biolabs). Forward primer: GATTAGATACCCTGGTAGTCCACGC; reverse primer: TCTCACGACACGAGCTGACGAC. The sequence of the gel purified DNA fragment was determined using both forward and reverse primers in separate sequencing reactions provided by the Eurofins Genomics (Germany) sequencing service. The resulting DNA sequence was searched in the 16S rRNA database (Bacteria and Archaea) subset at the National Center for Biotechnology using BLASTN 2.2.30 + .

3.4. Gas phase analyses

The concentrations of gaseous H_2S, CH_4, and CO_2 within the sewer pipe atmosphere were measured periodically, using a Draeger 3000 gas monitor. Long-term gas observations coupled with temperature records were conducted to monitor the inhibitory effect of $FeCl_2$ addition into the wastewater on gaseous H_2S emission. Therefore, several myDataSens1000_H_2S gas monitors were installed in consecutively positioned manholes, to monitor the H_2S concentrations over several weeks.

4. Results
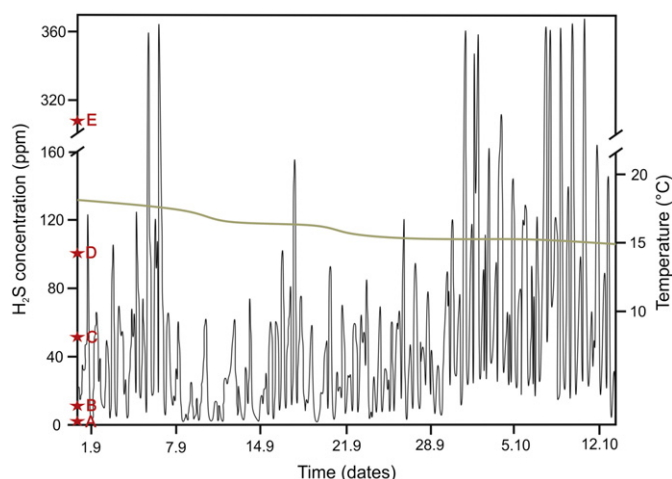
4.1. Wastewater chemistry—atmospheric sewer composition

Wastewater samples taken throughout the whole system showed a decrease in pH from 8.0 ± 0.2 within the storage basins (SB1 and SB2) down to 7.4 ± 0.3 within the sections of the gravity sewer (GS1 and GS2; Fig. 1). Consistently, the redox potential values from +51 mV (SB1) and +32 mV (SB2) decreased down to −248 mV (GS1) and −320 mV (GS2), indicating the progressive evolution from oxidizing to strongly reducing conditions within the wastewater. Occurring re-oxidation could be quantified within GS1, where O_2 concentrations increased from 1.4 mg l^{-1} in the first manhole (GS1-1) up to 4.3 mg l^{-1} within SB2. Interestingly, the O_2 concentrations at SB1 were extremely low, between 0.2 and 0.8 mg l^{-1}. In SB1, sulfate concentrations from 64 to 115 mg l^{-1} were measured, which decreased down to 25 ± 15 mg l^{-1} of SO_4^{2-} in the first manholes of GS1 after the upper power main (PM1) of the system. In GS1 the SO_4^{2-} concentration within the wastewater increased continuously with flow distance. Finally, in SB2, concentrations between 23 and 249 mg l^{-1} of SO_4^{2-} were analyzed. After the second power main (PM2), low SO_4^{2-} concentrations of 30 ± 15 mg l^{-1} occurred again. Sulfide concentrations of 0.35 mg l^{-1} were measured within SB1, which decreased after the PM1 down to 0.06 mg l^{-1}. Individual concentrations of dissolved components in the wastewater are displayed in Table 1.

Fig. 2. Typical evolution of concentrations of gaseous H_2S within the 4th manhole (GS-1-4) of GS1 (gray line). Internal manhole temperature is displayed in green colour. Red stars (A-E) mark important H_2S thresholds for human beings, such as odor threshold (A), eye irritation and headache (B), severe damages of eyes and respiratory systems (C), emerging odorless for human beings (D) and possible death (E) [7].

The data of long term gas measurements showed average concentrations of 6 ppm of H_2S, with large variations between 0.1 and 367 ppm, within the 4th manhole of GS1 (GS1-4) during $FeCl_2$ addition over a 6 week period (closed lid). Without the $FeCl_2$ addition, the H_2S concentrations at least doubled. The typical H_2S long term concentration, concurrent temperature variations and critical H_2S thresholds for the human beings are presented in Fig. 2. The gas measurements, conducted during sampling within different manholes, displayed concentrations up to 84 ppm of H_2S (open lids). With the flow direction of the wastewater a decrease in gaseous H_2S concentrations was detected, resulting in manholes without any recognizable H_2S emission at the end of GS1 and GS2. Indeed, high CO_2 concentrations of up to 2600 ppm (typical atmospheric CO_2 around 370 ppm) were measured throughout the whole system. Additionally, CH_4 concentrations of up to 1760 ppm were reached in the first few manholes after the two power mains.

4.2. Sulfuric acid attack and concrete corrosion

Drill cores, extracted from the most heavily corroded manholes in the upper sections of GS1 and GS2, revealed mean corrosion rates of 0.4 cm yr^{-1} (Table 2). Significant higher maximum corrosion rates of up to >1.0 cm yr^{-1} were reached in certain strongly deteriorated manholes, e.g. GS2-1.

The intact precast concrete of drill cores, extracted from the manholes of GS1 and GS2, showed compressive strengths of 88 ± 11 N/mm^3 and residual thickness of 4.0 to 12.5 cm. Therefore, the loss of material within the heavily corroded manholes could be determined with up to 9 cm within the last 9 years. Mineral compositions of intact concrete were quantified and subsequently compared to compositions of

Table 1
Wastewater chemistry along the flow direction within the sewer system. Samples were gathered from the two storage basins (SB1 and SB2) as well as from the first (GS1-1), 6th (GS1-6-6) and 7th manhole of gravity sewer 1 (GS1-7-2), and from the first manhole of gravity sewer 2 (GS2-1-6). Temperature (T°C), pH, electric conductivity (EC) and redox potential (Eh) were measured directly after sampling. Additionally, concentrations of dissolved organic carbon (DOC) are displayed. Complete concentrations of cations (Na$^+$, NH$_4^+$, K$^+$) and anions (Cl$^-$, PO$_4^{3-}$) are displayed within the Appendix A.

Sample ID	pH	T °C	EC mS cm^{-1}	Eh mV	O_2 mg l^{-1}	SO_4^{2-} mg l^{-1}	Ca^{2+} mg l^{-1}	Mg^{2+} mg l^{-1}	DOC mg l^{-1}
SB1-5	8.2	10.0	1.7	51.0	0.8	74.3	65.2	13.9	73.0
GS1-1	7.4	8.0	1.7	−157	1.4	41.2	74.6	14.9	64.5
GS1-6-5	7.4	17.7	1.4	−209	1.6	23.3	66.9	12.2	56.2
GS1-7-2	7.3	9.1	1.5	−248	1.8	152	114	13.2	83.0
SB2-2	7.8	9.6	1.8	32.0	4.3	249	147	14.3	83.0
GS2-1-6	7.6	13.5	0.9	−320	0.5	28.7	49.3	9.90	27.5

Table 2
Characteristics of drill cores taken from heavily damaged concrete manholes (N_{dc} = number of cores extracted) showing various states of concrete corrosion. The residual thickness (L_{dc}) of each altered concrete liner was directly measured and compared with that of unaltered concrete (13.0 cm) to achieve corrosion rates in cm yr^{-1}(R_c) and the loss of material (ML). The depth of the different manholes (shaft depth), the compression strength (CS) and density ($\rho_{concrete}$) of the drill cores extracted is additionally reported.

Manhole ID	shaft depth cm	CS N/mm^2	$\rho_{concrete}$ kg/m^3	N_{dc}	L_{dc} cm	ML cm	R_c cm yr^{-1}
GS1-4	290	85.1	2370	4	8.5; 9.5; 9.0; 10.0	4.5; 3.5; 4.0; 3.0	0.5; 0.4; 0.4; 0.3
GS1-6	315	97.9	2410	2	9.0; 11.0	4.0; 2.0	0.4; 0.2
GS1-7	273	70.5	2340	2	11.0; 11.5	2.0; 1.5	0.2; 0.2
GS1-26	260	79.9	2330	2	10.0; 12.0	3.0; 1.0	0.3; 0.1
GS1-29	220	90.0	2390	2	12.5; 12.5	0.5; 0.5	0.1; 0.1
GS1-32	170	83.4	2310	2	12.0; 12.5	1.0; 0.5	0.1; 0.1
GS2-1-2	264	106.2	2390	6	4.0; 5.0; 5.0; 6.5; 7.0; 9.5	9.0; 8.0; 8.0; 6.5; 6.0; 3.5	1.0; 0.9; 0.9; 0.7; 0.7; 0.4
GS2-2	274	97.8	2380	1	11.0	2.0	0.2

altered concrete. The siliceous compounds of the aggregates remained largely unaffected by corrosion, while the carbonatic aggregates were almost completely dissolved or transformed. Analogous, the latter is valid for the cementitious phases, mainly calcium–silicate–hydrate phases (C–S–H) and portlandite (Ca(OH)$_2$). The alteration of Ca-bearing mineral phases yielded in the precipitation of large quantities of gypsum of up to 42 wt.%. Additionally, significant amounts of anhydrite (CaSO$_4$; 16 ± 1 wt.%) and bassanite (CaSO$_4$ · 0.5H$_2$O; 3 ± 2 wt.%) formed within the corrosion layer of the first two corroded manholes of GS1 (GS1-3 and GS1-4) and the first manhole of GS2 (GS2-1). The change in the quantitative, mineralogical composition of unaltered concrete into strongly deteriorated concrete layers is displayed in Table 3.

The amount of TOC in the deteriorated concrete ranged between 0.12 and 0.51 wt.%, while TOC quantities between 0.09 and 0.25 wt.% were analyzed for non-deteriorated, respectively.

Microprobe analyses clearly displayed proceeding transformation of the cementitious matrix into gypsum, as well as continuing dissolution and leaching of the cementitious phases. Carbonate aggregates were gradually dissolved and transformed into gypsum, whereas, within GS1-3, GS1-4 and GS2-1 additional anhydrite and bassanite formation occurred. Secondary electron images (SEI) clearly showed gypsum formation within the deteriorated cementitious matrix (Fig. 3). The residuals of the aggregates, mainly quartz, feldspar (plagioclase and K-feldspar) and mica (muscovite/biotite) as well as distinct Fe-bearing phases like ferrohornblende ((Ca$_2$Fe$_5$Al(SiAlO$_{22}$)(OH)$_2$) and ilmenite (TiFeO$_3$) remained unaltered. A sharp transition zone (width about 100 μm) can be seen between the initial pristine concrete and highly altered cementitious matrixes, displaying massive occurrences of gypsum, bassanite and anhydrite (Fig. 4).

Interstitial solutions, extracted from the deteriorated concrete, showed extremely low pH values between 0.7 and 3.1, while concentrations of SO$_4^{2-}$ reached high values between 2 and 104 g l^{-1}. Additionally, high concentrations of Ca^{2+} (550 ± 100 mg l^{-1}), Mg^{2+} (52 to 4321 mg l^{-1}) and NH$_4^+$ (63 to 2994 mg l^{-1}) were measured. In general, a strong and positive correlation between a decrease in pH and elevated dissolved ion concentrations is evident. The Ca-concentration does not follow this trend, but displayed quite constant concentrations. All interstitial solutions were saturated with respect to gypsum (SI$_{Gp}$ between 0.02 and 0.41) and anhydrite (SI$_{Anh}$ between 0.01 and 0.43) while being slightly under-saturated with respect to bassanite (SI$_{Bs}$ between −0.94 and −0.52). Typical enrichment trends in dissolved components, as well as saturation indices for relevant sulfate minerals are summarized in Table 4.

Bacteria, enriched from deteriorated concrete samples, were isolated and identified as SOB belonging to the species *A. thiooxidans*. The sequenced 16S rDNA fragment was 99.6% identical to the sequence of *A. thiooxidans* ATCC 19377 (database entry NR_044920.1). A search against NCBI´s (Nacional Center for Biotechnology Information) complete non-redundant nucleotide collection revealed several hits with 100% sequence identity to 16sDNA fragments from uncultured bacteria (e.g. accession number KF845940) present in biofilms associated with concrete corrosion in the USA, for instance a 98.5% genetic conformity was determined for *A. ferrooxidans* [33].

5. Discussion

The results obtained in the present case study verified that the underlying mechanisms of concrete corrosion are attributed to microbial induced concrete corrosion (MICC). Measured redox potentials down
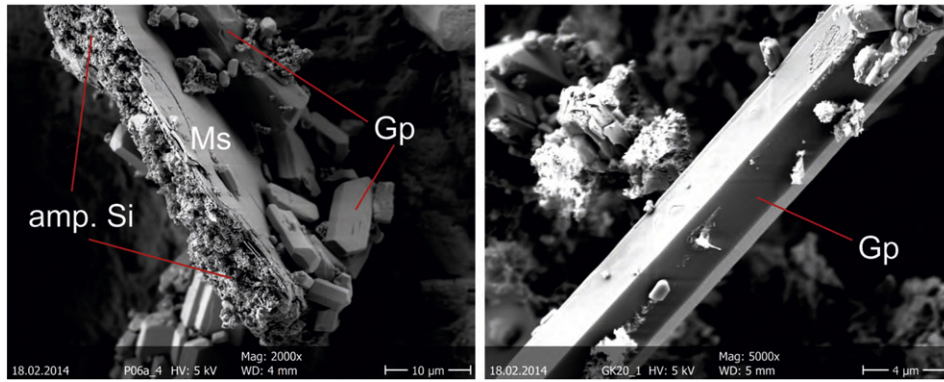
Table 3
Mineralogical composition of concrete samples of non-corroded concrete from drill cores, as well as of corroded areas obtained by Rietveld refinement of powder XRD patterns in wt.%, containing quartz (Qz), plagioclase (Pl), alkali feldspar (Kfs), calcite (Cal), muscovite (Ms), portlandite (Port), hornblende (Hbl), clinochlore (Clc), gypsum (Gp), bassanite (Bs), anhydrite (Anh), and x-ray amorphous phases (Amph).

	Sample ID	Qz	Pl	Kfs	Cal	Ms	Port	Hbl	Clc	Gp	Bs	Anh	Amph	R_{wp}
Intact	GS1-4-4	41.3	20.2	6.7	5.4	5.2	1.8	0.0	0.7	0.9	0.0	0.0	17.9	5.79
	GS1-6-2	42.2	19.4	4.9	6.8	4.8	2.4	1.4	1.0	0.0	0.0	0.0	17.1	5.54
	GS1-7-2	44.2	13.6	3.3	6.8	4.3	1.6	0.6	0.6	1.2	0.0	0.0	23.9	5.38
	GS1-25-2	40.7	13.5	3.9	9.7	4.5	2.0	1.1	0.4	2.7	0.0	0.0	22.5	5.33
	GS1-28-2	40.2	18.4	5.6	6.7	3.9	1.1	1.4	0.0	2.2	0.0	0.0	20.4	5.34
	GS1-31-2	37.0	15.4	4.4	12.9	4.1	2.7	0.0	0.7	0.6	0.0	0.0	22.2	5.44
	GS2-1-3	41.3	14.1	3.3	12.1	3.9	2.2	1.7	0.7	0.6	0.0	0.0	20.1	5.35
	GS2-2-1	38.9	15.6	5.8	7.0	3.6	1.9	0.6	0.6	0.0	0.0	0.0	26.1	5.53
Corroded	GS1-3-1	27.2	6.6	2.8	0.0	0.0	0.0	0.0	0.0	25.5	1.5	15.2	11.6	7.02
	GS1-4-1	42.0	10.4	0.0	0.0	3.9	0.0	0.0	0.0	12.0	0.8	10.2	10.7	6.05
	GS1-5-1	32.7	13.6	6.6	0.0	0.0	0.0	8.3	0.0	27.8	0.0	0.0	10.7	7.41
	GS1-6-2	33.1	12.5	0.0	0.0	4.4	0.0	2.2	0.0	30.2	0.0	0.0	16.8	7.17
	GS1-8-1	34.0	18.8	0.0	0.0	0.0	0.0	0.0	0.0	33.8	0.0	0.0	12.9	7.18
	GS2-1-1	34.0	13.4	1.8	0.0	2.6	0.0	0.0	0.0	24.3	4.9	17.3	1.8	7.35
	GS2-1-2	31.4	14.5	0.0	0.0	0.0	0.0	0.0	0.0	43.0	0.0	0.0	10.8	7.14

Fig. 3. SE-images showing neo-formed gypsum (Gp) crystals due to propagating MICC, as well as amorphous silica (amp. Si) and relicts of mica such as muscovite (Ms).

to −320 mV as well as low oxygen levels in the wastewater clearly indicated prevailing anaerobic conditions and associated bacterial activity within PM1 and PM2. There, anaerobic autotrophic organisms, mainly of the genus *Desulfovibrus* and *Desulfobulbus*, oxidized organic matter using sulfate as the electron acceptor in the absence of oxygen and nitrate [3]. This process resulted in the formation of sulfide species, including H_2S, at prevailing pH values between 7 and 8. The sulfide production is accompanied by a significant decrease in the concentration of dissolved sulfate, from about 105 to 14 mg l^{-1}, throughout the power mains. Subsequently, H_2S was liberated from the wastewater into the manholes atmospheres, where concentrations of up to 367 ppm of

H_2S were reached. $FeCl_2$ addition has proven to trigger iron sulfide precipitation, e.g. FeS_2 and FeS, thus reducing H_2S concentrations down to an average value of 6 ppm. However, partial re-oxidation of metastable FeS into SO_4^{2-} ions within GS1 due to re-aeration resulted in elevated SO_4^{2-} concentrations of up to 247 mg l^{-1} within SB2. Subsequently, the sulfate ions are reduced within PM2 resulting in high sulfide production rates and consistently high H_2S emission within GS2-1. Concentrations of CO_2 up to 2600 ppm and CH_4 up to 1760 ppm were quantified in the sewer atmosphere. CH_4 is a common byproduct of methanogenesis, which typically proceeds under extremely reducing conditions that are validated by redox potentials below −200 mV
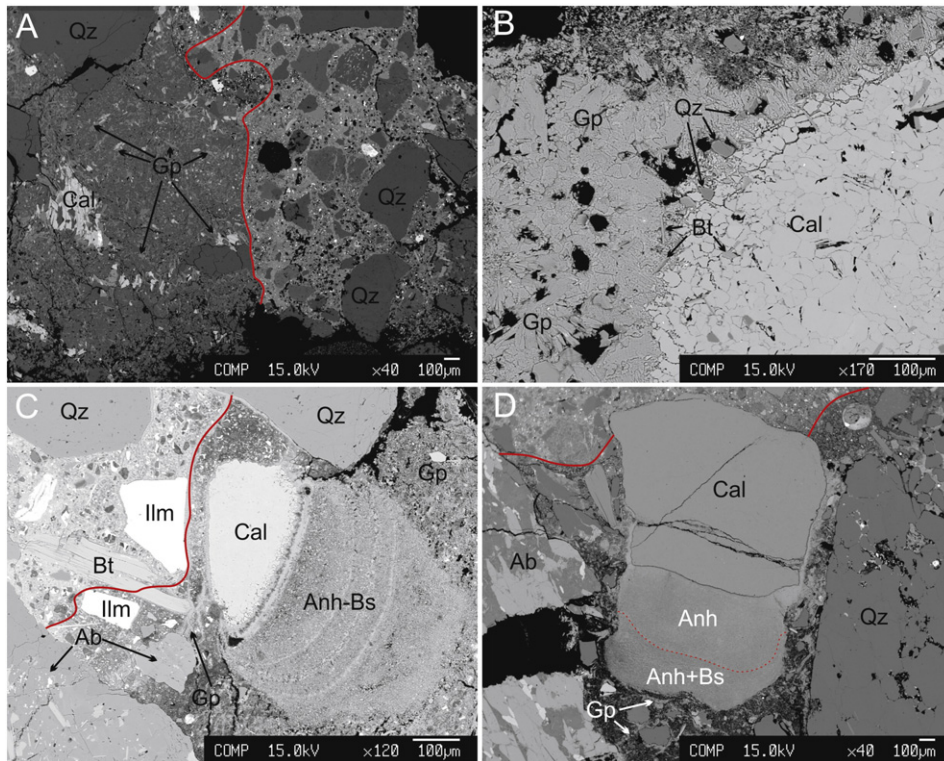

Fig. 4. BSE images of partly altered concrete. Top left (A) shows the sharp transition zone between strongly deteriorated concrete with abundant gypsum (Gp) on the left side and less altered concrete on the right side (red line). Top right (B) displays the gradual replacement of calcite (Cal) by gypsum (Gp). Bottom left (C) shows a corrosion front progressing from the right to the left side, causing dissolution of calcite and precipitation of gypsum, anhydrite (Anh) and bassanite (Bs), while grains of the additives like quartz (Qz), ilmenite (Ilm), biotite (Bt) and Albite (Ab) remain largely unaffected. Bottom left (D) displays an enlarged view of a calcite grain, which is transformed into anhydrite and bassanite. Gypsum occurs within the corroded matrix.

Table 4
Chemical composition of expressed interstitial solutions (PF) from strongly deteriorated concrete of GS1 and GS2. The pH and electrical conductivity (EC) were measured under laboratory conditions at 23 °C. Saturation indices (SI) for gypsum (Gp), bassanite (Bs) and anhydrite (Anh) were calculated using the computer code PHREEQC. The ion mass balance error (in %) is reported.

Sample ID	pH	EC mS cm⁻¹	Na⁺ mg l⁻¹	NH₄⁺ mg l⁻¹	K⁺ mg l⁻¹	Mg²⁺ mg l⁻¹	Ca²⁺ mg l⁻¹	Sr²⁺ mg l⁻¹	Cr mg l⁻¹	Fe mg l⁻¹	Zn mg l⁻¹	Al mg l⁻¹	F⁻ mg l⁻¹	Cl⁻ mg l⁻¹	NO₃⁻ mg l⁻¹	SO₄²⁻ mg l⁻¹	PO₄³⁻ mg l⁻¹	SI Gp	SI Bs	SI Anh	Error in %
GS1-3-PF1	0.9	59.5	97.8	296	122	115	680	5.88	24.5	1527	4.22	311	bdl.	44.6	29.0	13605	198	0.11	−0.84	0.10	−2.51
GS1-4-PF1	0.9	64.2	91	152	266	243	584	5.69	30.2	2080	3.47	540	bdl.	168	15.0	18139	156	0.14	−0.80	0.14	−2.38
GS1-5-PF1	2.4	5.7	182	80.8	33.3	51.8	577	3.26	1.90	151	1.58	21.2	bdl.	120	8.75	2719	0.89	0.06	−0.89	0.05	1.22
GS1-5-PF2	3.1	4.6	167	62.7	55.2	61.9	638	3.98	1.31	164	1.23	23	bdl.	112	11.7	2730	0.50	0.11	−0.84	0.10	−0.73
GS1-6-PF1	2.7	8.7	109	236	186	309	542	13.7	9.87	838	4.89	394	9.20	15.4	52.2	7127	3.74	0.10	−0.85	0.09	3.84
GS1-6-PF2	1.6	20.4	103	315	163	206	621	15.0	17.6	1005	3.90	305	5.23	15.9	45.1	9951	17.02	0.15	−0.80	0.14	0.95
GS1-6-PF3	2.3	11.3	100	341	194	343	508	8.10	43.0	1721	4.46	401	8.12	23.4	45.1	9436	15.08	0.10	−0.85	0.09	1.04
GS1-6-PF4	1.6	18.3	75.4	370	111	126	494	3.54	12.4	643	1.61	139	bdl.	20.8	28.5	7750	7.19	0.10	−0.91	0.03	−0.64
GS1-6-PF5	1.8	12.7	59.2	284	108	92.2	469	3.04	11.3	658	1.55	122	bdl.	17.0	22.4	6092	7.06	0.04	−0.94	0.01	−0.40
GS2-1-PF1	1.0	102.0	2978	2994	1383	4322	551	14.9	138	15693	152	5720	40.6	1648	6.58	104210	555	0.41	−0.52	0.43	5.79
GS2-1-PF2	1.1	69.5	404	635	534	1521	575	6.53	65.7	6241	70	1675	20.0	316	1.99	44090	345	0.23	−0.72	0.23	−0.87
GS2-1-PF3	0.7	101.0	573	210	330	990	567	4.54	48.1	2818	23	998	bdl.	376	5.35	40818	161	0.11	−0.83	0.11	2.16
GS2-1-PF4	0.9	66.4	523	198	346	931	520	8.47	59.6	2943	18	919	bdl.	380	3.85	32717	141	0.10	−0.85	0.09	−0.11

[26]. CH_4 production is reported in areas within the power main, where sulfate depletion occurred, indicating complete reduction of SO_4^{2-} into sulfide species within parts of PM1 and PM2 [34]. A schematic view of the main anaerobic microbial processes is given in Fig. 5.

The liberation of volatile components from the wastewater is controlled by the surrounding partial gas pressure, temperature and flow turbulences [5,13]. The latter seemed to engage in a central role concerning the degassing rapidity of the volatile components. Increased corrosion could be quantified in manholes of GS1 (GS1-3, GS1-4), where turns are enhancing flow turbulences and associated higher degassing rates of H_2S, CO_2 and CH_4. Moreover, after PM2 the wastewater entered GS2 two meters above the channel bottom, creating a waterfall. With increasing flow direction, a significant increased decline in H_2S concentrations within the atmosphere of the concrete based manholes was measured. Simultaneously, the highest corrosion rates of about 1 cm yr⁻¹ were measured in the first manhole of GS2 (GS2-1). Hence, in GS2 the intensities of cement corrosion decreased much faster with flow distance, compared to GS1 (Fig. 6).

After entering the sewer atmosphere within the manholes, H_2S was absorbed into the interstitial solutions of the outer layer of the concrete walls, where it oxidized through complex reaction paths [22,11], with H_2SO_4 being the final product. It is suggested that the uptake and transformation of gaseous H_2S into H_2SO_4 is more efficient in manholes with sealed covers, since the ventilation out of the manhole atmosphere is hampered and 100% water saturation within the pore structure of the concrete is reached, creating an environment similar to a bioreactor. Quantification of how much exactly the sealed covers attribute toward intensifying corrosion is difficult, since all of those strongly deteriorated manholes are situated within the first part of GS1 and GS2, where the most intensive degassing occurred simultaneously. However, no visible corrosion could be seen within the first two manholes of GS1 (GS1-1, GS1-2), which are coated with perforated covers, whereas the following strongly deteriorated manholes, (GS1-3 and following), matched those with sealed covers. Additionally, the straight course within this first 50 meters of GS1 promoted a calm wastewater flow with minor flow turbulences and consequential low degasification rates. During the early stages of the MICC attack carbonation due to the interaction between CO_2, condensed water, the calcium hydrate phases (C–H) and C–S–H phases of the cementitious matrix took place. Additionally, abiotic oxidation of H_2S occurred, producing thiosulfuric and polythionic acids [14]. Both processes reduced the pH from initially ~13 down to ~9.5. Below the latter pH, progressive colonization of aerobic heterotrophic bacteria results in biotic H_2SO_4 production. Through the ongoing decrease of pH different strains of neutrophile SOB colonized the pore system. Starting from pH 5, acidophil bacteria appeared. The bacteria extracted from the deteriorated concrete were identified as *A. thiooxidans*, which thrive until pH 0.2, if the sulfate concentrations exceed about 74 g l⁻¹ [35]. In our pore fluids the sulfate concentrations were up to 104 g l⁻¹.

It is likely that the bacteria *A. ferrooxidans* plays a central role in intensifying the corrosion rate of concrete in the present case study. These sulfur-oxidizing chemolithrophs have the ability to use ferric iron as an electron acceptor, if oxygen supply is limited. This ability potentially favors the production of H_2SO_4 in deeper, anoxic layers of the concrete, thereby accelerating the deterioration of the cementitious phases [36]. Huge amounts of dissolved iron of up to 15.6 g l⁻¹ were determined within the interstitial solution of deteriorated concrete (Table 4). The metabolism of *A. thiooxidans* and, most likely *A. ferrooxidans*, press ahead with the H_2SO_4 production and adherent concrete deterioration. According to Islander et. al. 1991 [14], only within this last stage of MICC, where acidophil bacteria are adopting the pore volume at pH below 5, intense concrete breakdown takes place. Considering higher corrosion rates as MICC progresses, it can be taken for granted that during the last years the corrosion rates within the system significantly exceeded the measured average rates of up to 1 cm yr⁻¹. This is due to the fact that the measured rates reflect the mean annual loss of the concrete wall material since the installation of the sewer
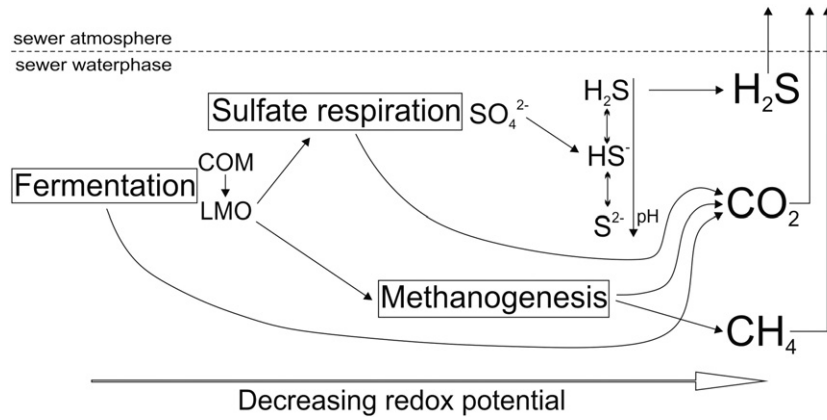
Fig. 5. Schematic view of the 3 microbial processes occurring under anaerobic conditions [20]. Initial transformation from complex organic molecules (COM) into low molecular organics (LMO) takes place through a series of reduction and oxidation processes. LMO are consumed by sulfate-reducing bacteria as well as methane-producing bacteria resulting in the formation of sulfide species, beside methane (CH_4) and CO_2 production. Note that each individual process is limited to a distinct redox potential.

system in 2004, whereas concrete alteration in the first years of service is considered low (Table 2). The measured TOC concentrations within the concrete of the initial precast elements confirm the application of superplasticizers, i.e. polycarbooxylate ether based superplasticizer (PCEs), which might promote the development of SOB by providing an additional carbon source for bacterial metabolism, beside of CO_2.

The produced H_2SO_4 triggered the dissolution of the cementitious matrix and carbonatic aggregates, as well as the neo-formation of gypsum, bassanite and anhydrite. In general, the degradation of the concrete can be assigned to coupled chemical reactions, as well as mechanical and microstructural processes (Fig. 6). Quantitative XRD analysis showed the gradual reduction of the C–S–H phases (amorphous content), portlandite and carbonates. The dissolution of these phases resulted in high concentrations of total dissolved solids and associated oversaturation of the interstitial solutions toward calcium sulfate minerals, thus triggering massive neo-formation of gypsum of up to 42 wt.%. Due to the proceeding dissolution of the supporting cementitious matrix, silica aggregates break

out, which caused a decrease in their abundances, although virtually not affected by MICC. The expected ettringite formation lacked due to its high solubility at the present low pH values and the fact that C_3A-reduced concrete was used in the concrete mixture. Bassanite and anhydrite formation within the most heavily corroded manholes (GS1-3, GS1-4 and GS2-1) could be explained by wetting and drying cycles and subsequent variable SO_4^{2-} and H_2O activities within the interstitial solutions of the concrete. According to Lawrence et. al. 1967 [37], transformation of gypsum into anhydrite occurs within a 4 molar H_2SO_4 solution at 1 atm pressure and 23 °C. Microprobe analysis support the concept of gradual depletion of the C–S–H phases within the cementitious matrix, adherent dissolution of portlandite and calcite, as well as massive Ca-mineral neo-formation due to propagating corrosion (Fig. 4). Moreover, progressing sulfate ion diffusion into the initially damaged concrete matrix is accompanied with a depletion of Si- and Mg-bearing cementitious phases, whereas Ca concentrations remained largely constant due to precipitation as (hydrated) Ca-sulfates. The mobilization and uptake of SO_4^{2-} ions proceeded along cracks and grain boundaries between the
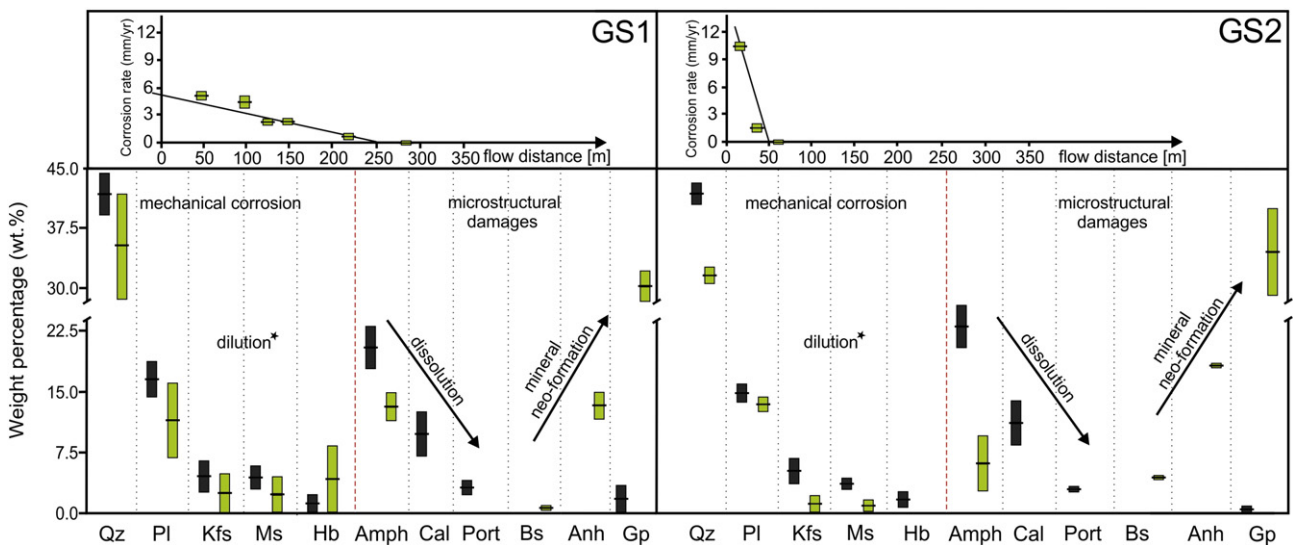
Fig. 6. Change in the quantitative, mineralogical composition of unaltered (grey) versus heavily damaged concrete (green), related to MICC. The concrete corrosion rate with flow distance within GS1 and GS2 is reported on top of the figure. Note the significantly highly localized concrete damage in GS2. *Ongoing dissolution of the supporting cementitious matrix is causing dilution of siliceous compounds such as quartz (Qz), plagioclase (Pl), K-feldspar (Kfs), muscovite (Ms) and hornblende (Hb). Decrease of carbonatic and cementitious phases like calcite (Cal) and portlandite (Port) can be attributed to dissolution and subsequent mineral neo-formation of gypsum (Gp), anhydrite (Anh) and bassanite (Bs) formation, which causes intense microstructural damage of the concrete. X-ray amorphous phases (Amph), mainly represent the CSH phases of the cement.

aggregates and the cement matrix, before propagating throughout the whole matrix.

Possible remediation strategies for the present case system are referred to the application of calcium aluminate cement (CAC) based concrete, as they show better performances in systems exposed to MICC, compared to OPC concrete [23,38,39]. Here, the composition of the applied cement plays a major role concerning the establishment of biofilms within the concrete pore volumes. The CAC reveals inhibitory effects on the activity of the neutrophile bacteria since Al is known to have bacteriostatic characteristics [40]. Additionally, the hydrated alumina phases react with the H_2SO_4, to form an alumina gel layer, which significantly decreases the porosity and permeability and hence the diffusion rates in particular within the concrete surface layers. Since the alumina gel layer forms instantaneously, significant lower H_2S diffusion rates, as well as lower oxygen penetration depths could be achieved, thereby limiting biofilm adhesion [39]. Furthermore, the higher acid neutralization capacity of $Al(OH)_3$ compared to Ca-hydroxide/ carbonate minerals decelerates the pH decrease of the concrete within corrosive environments. In this context, it is crucial to adapt the Austrian standards for sanitary engineering (e.g. ÖNORM B 2503 in Austria), which currently neither value critical H_2S_{gas} levels for constructive materials, nor other potentially relevant gaseous components, such as CO_2 and NH_3. Additionally, suggested C_3A-free concrete contains higher Fe_2O_3 contents, which might favor the development of A. ferrooxidans, thus increasing biotic H_2SO_4 production.

6. Summary and conclusion

In the present study, a multi proxy approach, including mineralogical, mechanical, chemical, and biological analyses, was used as a highly powerful tool to investigate the complex reaction mechanisms and controlling environmental parameters for progressing MICC. The deterioration of concrete in the studied Austrian sewer system was accordingly identified to be attributed to bacteriogenically induced sulfuric acid attack, associated with the formation and degassing of high quantities of H_2S. Long retention times of the wastewater within the power mains combined with sealed manhole covers and low discharge rates created 'bioreactor conditions', which resulted in high microbial activity, abundant sulfate reduction, subsequently H_2S degassing and H_2SO_4 production. H_2SO_4 accumulation in the interstitial solutions of the concrete resulted in pH values between 0.7 and 3.1. This extremely aggressive (micro) environment enhanced the dissolution of the cement matrix and in particular the breakdown of non-siliceous aggregates as well as the neo-formation of potentially expandable alteration products, i.e. gypsum, bassanite and anhydrite. In the present case, the expected ettringite formation lacked due to very low pH values and the application of C_3A-free concrete used for the concrete mixture. High concrete corrosion rates exceeding 1 cm y^{-1} were obtained, which caused large parts of the present sewer system to be strongly deteriorated after only 9 years of usage, although highly sulfate resistant concrete plus fly ash (w/c 0.35; C_3A-free cement) was applied.

Appendix A

A.1. Chemical composition of wastewater samples taken from different manholes within GS1 and GS2 as well as from SB1 and SB2. DOC: total dissolved organic carbon, where values are referred to wt. % of C.

Sample ID	Na^+ mg l^{-1}	NH_4^+ mg l^{-1}	K^+ mg l^{-1}	Mg^{2+} mg l^{-1}	Ca^{2+} mg l^{-1}	Cl^- mg l^{-1}	SO_4^{2-} mg l^{-1}	PO_4^{3-} mg l^{-1}	DOC mg l^{-1}
SB1-1	85.4	76.9	23.1	12.9	69.0	104	64.0	2.77	n.a.
SB1-4	72.9	85.4	21.4	13.0	83.7	90.4	115	0.45	61.1
SB1-5	142	104	24.9	13.9	65.2	237	74.3	1.84	73.0
GS1-1	136	73.3	25.9	14.9	74.6	228	41.2	6.34	64.5
GS1-6-1	39.6	23.5	8.62	4.76	27.3	46.3	14.3	3.88	82.5
GS1-6-2	37.3	22.7	8.26	4.86	38.0	43.8	41.4	3.97	59.4
GS1-6-3	28.6	41.3	9.55	7.91	27.7	25.9	21.5	8.02	56.2
GS1-6-4	93.4	56.8	25.2	11.2	71.5	102	40.9	7.80	n.a.
GS1-6-5	92.0	70.0	25.7	12.2	66.9	102	23.3	14.8	n.a.
GS1-6-6	68.6	50.4	18.3	10.1	79.4	87.3	79.7	8.13	50.2
GS1-6-7	67.9	50.0	18.0	9.75	70.5	86.4	51.0	9.43	48.0
GS1-6-8	70.8	58.6	18.4	10.8	73.0	94.3	57.2	7.23	46.2
GS1-6-9	138	74.9	23.9	15.2	73.6	223	48.8	5.32	65.0
GS1-7-1	95.5	70.9	23.6	13.2	81.5	89.7	64.4	18.6	83.7
GS1-7-2	95.9	70.3	24.3	13.2	114	91.0	152	16.8	83.0
GS1-8-1	27.9	28.2	9.21	6.71	26.3	29.9	15.4	4.03	52.4
SB2-1	34.8	23.5	8.18	4.82	30.3	40.2	23.3	3.55	38.7
SB2-2	110	83.9	32.9	14.3	147.5	104	249	15.3	83.0
GS2-1-1	36.3	25.3	8.38	5.18	28.2	43.5	13.8	5.09	56.5
GS2-1-2	77.9	68.3	24.1	17.0	77.4	85.2	45.0	10.5	n.a.
GS2-1-5	60.9	51.1	20.8	10.1	49.9	64.1	30.8	11.3	25.5
GS2-1-6	59.5	49.9	20.1	9.87	49.3	62.8	28.7	11.2	27.5
GS2-1-7	94.9	70.9	21.0	13.2	76.2	89.1	44.4	19.0	73.2
GS2-1-8	94.0	71.6	21.2	13.0	69.7	88.6	23.8	19.4	77.3
GS2-1-9	152	77.4	22.6	14.3	63.8	214	32.0	11.1	69.2

n.a. = not analyzed.

References

[1] M.G.D. Gutiérrez-Padilla, A. Bielefeldt, S. Ovtchinnikov, M. Hernandez, J. Silverstein, Biogenic sulfuric acid attack on different types of commercially produced concrete sewer pipes, Cem. Concr. Res. 40 (2010) 293–301, http://dx.doi.org/10.1016/j.cemconres.2009.10.002.

[2] M. O'Connell, C. McNally, M.G. Richardson, Biochemical attack on concrete in wastewater applications: A state of the art review, Cem. Concr. Compos. 32 (2010) 479–485, http://dx.doi.org/10.1016/j.cemconcomp.2010.05.001.

[3] H.S. Jensen, Hydrogen sulfide induced concrete corrosion of sewer networks(PhD thesis) Aalborg University, 2009.

[4] A.P. Joseph, J. Keller, H. Bustamante, P.L. Bond, Surface neutralization and H(2)S oxidation at early stages of sewer corrosion: influence of temperature, relative humidity and H(2)S concentration, Water Res. 46 (2012) 4235–4245, http://dx.doi.org/10.1016/j.watres.2012.05.011.

[5] E. Saracevic, Zur Kenntnis der Schwefelwasserstoffbildung und -vermeidung in Abwasserdruckleitungen(PhD thesis) TU Wien, 2008.

[6] World Health Organisation, Hydrogen Sulfide, Air Qual. Guidel. Eur., Copenhagen 2000, p. 7 (http://www.euro.who.int/__data/assets/pdf_file/0005/74732/E71922.pdf).

[7] WHO, Air Quality Guidelines 40 (2001) 9823, http://dx.doi.org/10.1002/1521-3773(20010316)40:6<9823::AID-ANIE9823>3.3.CO;2-C.

[8] W.M. Olmstead, H. Hamlin, Converting portions of the Los Angeles outfall sewer into a septic tank, Eng. News (1900) 971–980.

[9] H.T. Dinh, J. Kuever, M. Mußmann, A.W. Hassel, Iron corrosion by novel anaerobic microorganisms, Nature (2004) 829–832, http://dx.doi.org/10.1038/nature02349.1.2.3.4.5.6.7.8.9.10.Wilson.

[10] T. Hvitved-Jacobsen, J. Vollertsen, C. Yongsiri, A.H. Nielsen, Sewer microbial processes, emissions and impacts, Sewer Process, Networks, Paris 2002, p. 13.

[11] M. Alexander, A. Bertron, N. De Belie, Performance of Cement-Based Materials in Aggressive Aqueous Environments, 1st ed. Springer, Ghent, 2013.http://dx.doi.org/10.1007/978-94-007-5413-3.

[12] J. Tritthart, Chloride binding in cement I. Investigations to determine the composition of porewater in hardened cement, Cem. Concr. Res. 19 (1989) 586–594.

[13] H.S. Jensen, P.N.L Lens, J.L. Nielsen, K. Bester, A.H. Nielsen, T. Hvitved-Jacobsen, et al., Growth kinetics of hydrogen sulfide oxidizing bacteria in corroded concrete from sewers, J. Hazard. Mater. 189 (2011) 685–691, http://dx.doi.org/10.1016/j.jhazmat.2011.03.005.

[14] B.R.L. Islander, J.S. Devinny, A. Member, F. Mansfeld, A. Postyn, H. Shih, Microbial ecology of crown corrosion in sewers, J. Environ. Eng. 117 (1992) 751–770.

[15] A.H. Nielsen, J. Vollertsen, H.S. Jensen, T. Wium-Andersen, T. Hvitved-Jacobsen, Influence of pipe material and surfaces on sulfide related odor and corrosion in sewers, Water Res. 42 (2008) 4206–4214, http://dx.doi.org/10.1016/j.watres.2008.07.013.

[16] A. Yousefi, A. Allahverdi, P. Hejazi, Accelerated biodegradation of cured cement paste by Thiobacillus species under simulation condition, Int. Biodeterior. Biodegrad. 86 (2014) 317–326, http://dx.doi.org/10.1016/j.ibiod.2013.10.008.

[17] L. Zhang, P. De Schryver, B. De Gusseme, W. De Muynck, N. Boon, W. Verstraete, Chemical and biological technologies for hydrogen sulfide emission control in sewer systems: a review, Water Res. 42 (2008) 1–12, http://dx.doi.org/10.1016/j.watres.2007.07.013.

[18] S. Soleimani, O.B. Isgor, B. Ormeci, Resistance of biofilm-covered mortars to microbiologically influenced deterioration simulated by sulfuric acid exposure, Cem. Concr. Res. 53 (2013) 229–238, http://dx.doi.org/10.1016/j.cemconres.2013.06.016.

[19] F. Mittermayr, M. Rezvani, A. Baldermann, S. Hainer, P. Breitenbücher, J. Juhart, et al., Sulfate resistance of cement-reduced eco-friendly concretes, Cem. Concr. Compos. 55 (2015) 364–373, http://dx.doi.org/10.1016/j.cemconcomp.2014.09.020.

[20] G. Jiang, E. Wightman, B.C. Donose, Z. Yuan, P.L. Bond, J. Keller, The role of iron in sulfide induced corrosion of sewer concrete, Water Res. 49 (2014) 166–174, http://dx.doi.org/10.1016/j.watres.2013.11.007.

[21] D. Nica, G. Zuo, J. Davis, Quantifying microbially induced deterioration of concrete: initial studies, Int. Biodeterior. Biodegrad. 49 (2002) 227–234, http://dx.doi.org/10.1016/S0964-8305(02)00049-5.

[22] N. De Belie, J. Monteny, A. Beeldens, E. Vincke, D. Van Gemert, W. Verstraete, Experimental research and prediction of the effect of chemical and biogenic sulfuric acid on different types of commercially produced concrete sewer pipes, Cem. Concr. Res. 34 (2004) 2223–2236, http://dx.doi.org/10.1016/j.cemconres.2004.02.015.

[23] J. Herisson, E.D. van Hullebusch, M. Moletta-Denat, P. Taquet, T. Chaussadent, Toward an accelerated biodeterioration test to understand the behavior of Portland and calcium aluminate cementitious materials in sewer networks, Int. Biodeterior. Biodegrad. 84 (2013) 236–243, http://dx.doi.org/10.1016/j.ibiod.2012.03.007.

[24] A. Eštokov, V.O. Harbuľáková, A. Luptáková, N. Števulová, Study of the Deterioration of Concrete Influenced by Biogenic Sulphate Attack, Procedia Eng. 42 (2012) 1731–1738, http://dx.doi.org/10.1016/j.proeng.2012.07.566.

[25] A.H. Nielsen, J. Vollertsen, H.S. Jensen, H.I. Madsen, T. Hvitved-Jacobsen, Aerobic and Anaerobic Transformations of Sulfide in a Sewer System – Field Study and Model Simulations, Proc. Water Environ. Fed. 2006 (2006) 3654–3670, http://dx.doi.org/10.2175/193864706783751447.

[26] T. Hvitved-Jacobsen, J. Vollertsen, A.H. Nielsen, Sewer Processes - Microbial and Chemical Process Engineering of Sewer Networks, Second ed. CRC Press, London, 2013.

[27] D. Cline, J, Spectrophotometric determination of hydrogen sulfide in natural waters, Limnol. Oceanogr. 14 (1969) 454–458.

[28] N. Kowalski, O. Dellwig, M. Beck, M. Grunwald, C.-D. Dürselen, T.H. Badewien, et al., A comparative study of manganese dynamics in the water column and sediments of intertidal systems of the North Sea, Estuar. Coast. Shelf Sci. 100 (2012) 3–17, http://dx.doi.org/10.1016/j.ecss.2011.03.011.

[29] D.L. Parkhurst, C.A.J. Apello, User's guide to PHREEQC (V2), 1999. 312.

[30] F. Mittermayr, A. Baldermann, C. Kurta, T. Rinder, D. Klammer, A. Leis, et al., Evaporation — a key mechanism for the thaumasite form of sulfate attack, Cem. Concr. Res. 49 (2013) 55–64, http://dx.doi.org/10.1016/j.cemconres.2013.03.003.

[31] R.L. Starkley, Isolation of some bacteria which oxidize thiosulfate, Soil Sci. 39 (1935) 197–220.

[32] S. Chakravorty, D. Helb, M. Burday, N. Connell, D. Alland, A detailed analysis of 16S ribosomal RNA gene segments for the diagnosis of pathogenic bacteria, J. Microbiol. Methods 69 (2007) 330–339.

[33] A.L. Ling, C.E. Robertson, N.R. Pace, M.T. Hernandez, Microbial and Chemical Characterization of Concrete Corrosion Biofilms of Wastewater Infrastructure in Ten Cities, (Unpublished). (n.d.).

[34] T.E. Cappenberg, Interrelations between sulfate-reducing and methane-producing bacteria in bottom deposits of a fresh-water lake, J. Microbiol. 40 (1974) 285–295.

[35] E.Y. Lee, N.Y. Lee, K.-S. Cho, H.W. Ryu, Removal of hydrogen sulfide by sulfate-resistant Acidithiobacillus thiooxidans AZ11, J. Biosci. Bioeng. 101 (2006) 309–314, http://dx.doi.org/10.1263/jbb.101.309.

[36] D.E. Rawlings, D. Dew, C. Plessis, Biomineralization of metal-containing ores and concentrates, 7799 (2002) 4–5.

[37] L.A. Hardie, The gypsum-anhydrite equilibrium at one atmosphere pressure, Am. Mineral. 52 (1967).

[38] J. Herisson, M. Guéguen-Minerbe, E.D. van Hullebusch, T. Chaussadent, Behaviour of different cementitious material formulations in sewer networks, Water Sci. Technol. 69 (2014) 1502–1508, http://dx.doi.org/10.2166/wst.2014.009.

[39] J. Herisson, M. Gueguen-Minerbe, E.D. Van Hullebusch, T. Chaussadent, Biogenic corrosion mechanism: Study of parameters explaining calcium aluminate cement durability, Calcium Aluminates, Balkema 2014, pp. 645–658.

[40] A.M. Goyns, M. Alexander, Performance of various concretes in the Virginia experimental sewer over 20 years, Calcium Aluminates, Balkema 2014, pp. 573–584.